

## **3D model construction of induced polarization and resistivity data with quantifying uncertainties using geostatistical methods and drilling (Case study: Madan Bozorg, Iran)**

K. Mostafaei and H.R. Ramazi\*

*Faculty of Mining and Metallurgical Engineering, Amirkabir University of Technology, Tehran, Iran*

Received 3 March 2018; received in revised form 9 May 2018; accepted 3 June 2018

\*Corresponding author: ramazi@aut.ac.ir (H.R.Ramazi).

### **Abstract**

Madan Bozorg is an active copper mine located in NE Iran, which is a part of the very wide copper mineralization zone named Miami-Sabzevar copper belt. The main goal of this research work is the 3D model construction of the induced polarization (IP) and resistivity (Rs) data with quantifying the uncertainties using geostatistical methods and drilling. Four profiles were designed and surveyed using the CRSP array based on the boreholes. The data obtained was processed, 2D sections of IP and Rs were prepared for each profile by inverting the data, and these sections were evaluated by some exploratory boreholes in the studied area. Based on the geostatistical methods, 3D block models were constructed for the 2D IP and Rs data, and the uncertainties in the prepared models were obtained. The mineralization location was determined according to the geophysical detected anomalies. In order to check the models, some locations were proposed for drilling in the cases that the borehole data was unavailable. The drilling results indicated a high correlation between the identified anomalies from the models and mineralization in the boreholes. The results obtained show that it is possible to construct 3D models from surveyed 2D IP & Rs data with an acceptable error level. In this way, the suggested omitted drilling locations were optimized so that more potentials could be obtained for copper exploration by the least number of boreholes.

**Keywords:** *3D Model, Induced Polarization, Resistivity, Geostatistics, Uncertainties, Drilling.*

### **1. Introduction**

Geophysical exploration is a part of geophysical methods used to measure the physical properties of bodies or rocks, and in particular, to identify the measurable differences between rocks with or without ore deposits or hydrocarbons. Exploration geophysics can be used to detect the target style of mineralization via measuring its physical properties directly [1]. Identification of contrasts in different physical properties of materials is the base of the geophysical methods [2]. In a mineral deposit, exploration depends on the physical properties of the target and its accompanied rock geological setting, and even its topographic geophysical method(s) are selected. In many cases, in order to achieve more certain results, integration of the methods is necessary [3]. Due to

optimization in cost and time, the application of geophysical exploration methods has recently been increasing in the mineral exploration investigation. The integrated geophysical methods are commonly used in mineral exploration to obtain qualified results [4]. In the mineral exploration of ores located in basement rocks, geophysical tools including different techniques such as induced polarization (IP) and resistivity (Rs) are important techniques [5]. The IP & Rs methods are among the geophysical methods applied in the subsurface study to assess the potential of mineral exploration. The goals of the IP and Rs methods are the selection of the best drilling points for exploration purposes [6].

Due to its low cost and time operation and also its limited damages to the environment, a combination of the IP and electrical Rs methods have been widely used in various mineral exploration studies such as polymetal in China [7], porphyry copper in Mexico [8], manganese in Iran [3], mineralization in Ethiopia [9], lenses of water-saturated unfrozen rocks (taliks) [10], Cu-dominated VHMS sulfate in Iran [4], and gold-silver deposit [11] and bitumen exploration in Iran [12].

A combination of the IP and electrical Rs methods has also been widely and fruitfully carried out in various geoscience fields, for example, the following environmental issues: prediction of pyrite oxidation and pollutant leaching associated with a coal washing waste dump in Iran [13]; delineate acid rock drainage pathways in gold mine [14]; study of AMD generation at the Haveri Au-Cu mine tailings, SW Finland [15]; mapping the flow pathways and contaminant transportation around a coal washing plant in Iran [16]; engineering geology; and mapping of lithotypes in a landfill site in Denmark [17].

In most earth science studies, interpolation is done after data gathering. As far as the numerical modeling of the geoscience data in un-sampled areas is concerned, interpolation is a method of constructing new data points within the range of a discrete set of known data points. In fact, the points between and around the available data would be estimated using interpolation. The interpolation methods are divided into two main parts: classic statistical and geostatistical methods. Versus the classical statistics, the geostatistical methods take into account the spatial variability of the target parameter in order to provide realistic spatial estimates together with a quantification of the associated uncertainty [18]. Spatial correlation data including distance and direction can be expressed in mathematical form, considering the spatial structure. This spatial structure is studied by means of a variogram in geostatistics [19].

The geostatistical technique was originally developed to estimate the regionalized variables such as the grade of an ore body at a known location in space, given a set of observed data. The regionalized variables are variables typical of a phenomenon developing in space (and/or time) and possessing a certain structure [20]. The geostatistical techniques are used a lot in geophysical investigations [18]. Many studies in the field of geophysical data analysis have been done using the geostatistical methods; the following studies can be cited: [19-24]. These

studies had good results but they also had weaknesses that can be mentioned as what follow. Since the geophysical modeling is concerned, a vast majority of studies have been carried out for the one- and two-dimensional models, while the 3D models are more convenient and reliable for the exploration drilling purposes. Calculating errors and uncertainties of the estimation obtained also plays a significant part for which there have been few studies that quantify them. Apart from the mentioned issues, the classification and prioritizing estimated blocks can numerically be quantified, and the errors that can decrease the risk of exploration (e.g. drilling) have not been prioritized. The fractal and multiracial models have also been applied to separate the anomalies from the background. The concept of fractals given by Mandelbrot (1983) has been applied in various fields. The choice of method depends upon the nature of data and purpose of the study. Due to the data, the "concentration-area" method has been used in this research work [6]. In the concentration-area fractal method, this subject present that the fractal dimension of various groups are different, i.e. mean anomaly is different from the fractal dimension of background.

In this research work, at first, the IP and Rs efficiency was investigated in the Madan Bozorg copper mine in detailed exploration and mining stages. For this purpose, a geophysical survey design was carried out based on the borehole exploration data. The data obtained was processed, and 2D sections of IP and Rs were prepared for each profile by inverting the data using the RES2DINV software. The correlation between IP, Rs, and copper mineralization has been checked out in the locations using exploratory boreholes in the two profile location. Collecting data in 3D mode is not possible in many situations due to the limitations in time, budget, surveying, geological, and topographical situations. Thus correctly extracting the 3D models out of 2D surveying is logical and useful in exploration operation. In this work, geophysical surveying was carried out by the CRSP-Combined Resistivity Sounding and Profiling-array, i.e. 2D array. A 3D model of data in this work was compiled according to the geostatistical methods. The uncertainties of the prepared models were obtained by geostatistical relationships. Finally, the accuracy of the constructed models was checked by drilling results.

## 2. Material and method

**2.1. Studied area- Madan Bozorg copper mine**

The Madan Bozorg copper mine is an active mine that is located 70 km east of Miami, Semnan Province, NE Iran; it is located 10 km north of the Abassabad village. The location map and access roads are presented in Figure 1.

From the geological viewpoint, Madan Bozorg is a part of a wide mineralization belt named Miami-Sabzevar copper belt. There are many lithology units in the entire Miami-Sabzevar copper belt but 2 main geological units, i.e. igneous rocks (porphyritic andesite and trachyandesite) and sedimentary rocks (limestone with marl), are more important. Mineralization has occurred in the

contact of andesite and limestone. The geology map of Madan Bozorg is presented in Figure 2. Based on this map, there are some lithology units including porphyritic trachyandesite, conglomerate, limestone, sandstone, and shale. There is a Quaternary alluvium in some locations. The sedimentary rocks consist of limestone, and in some parts, the mineral clay value increased and converted to marl. Mineralogy studies shows that limestone is a geochemistry barrier. Limestone cause the deposition of copper minerals so mineralization has occurred in the contact of andesite and limestone.

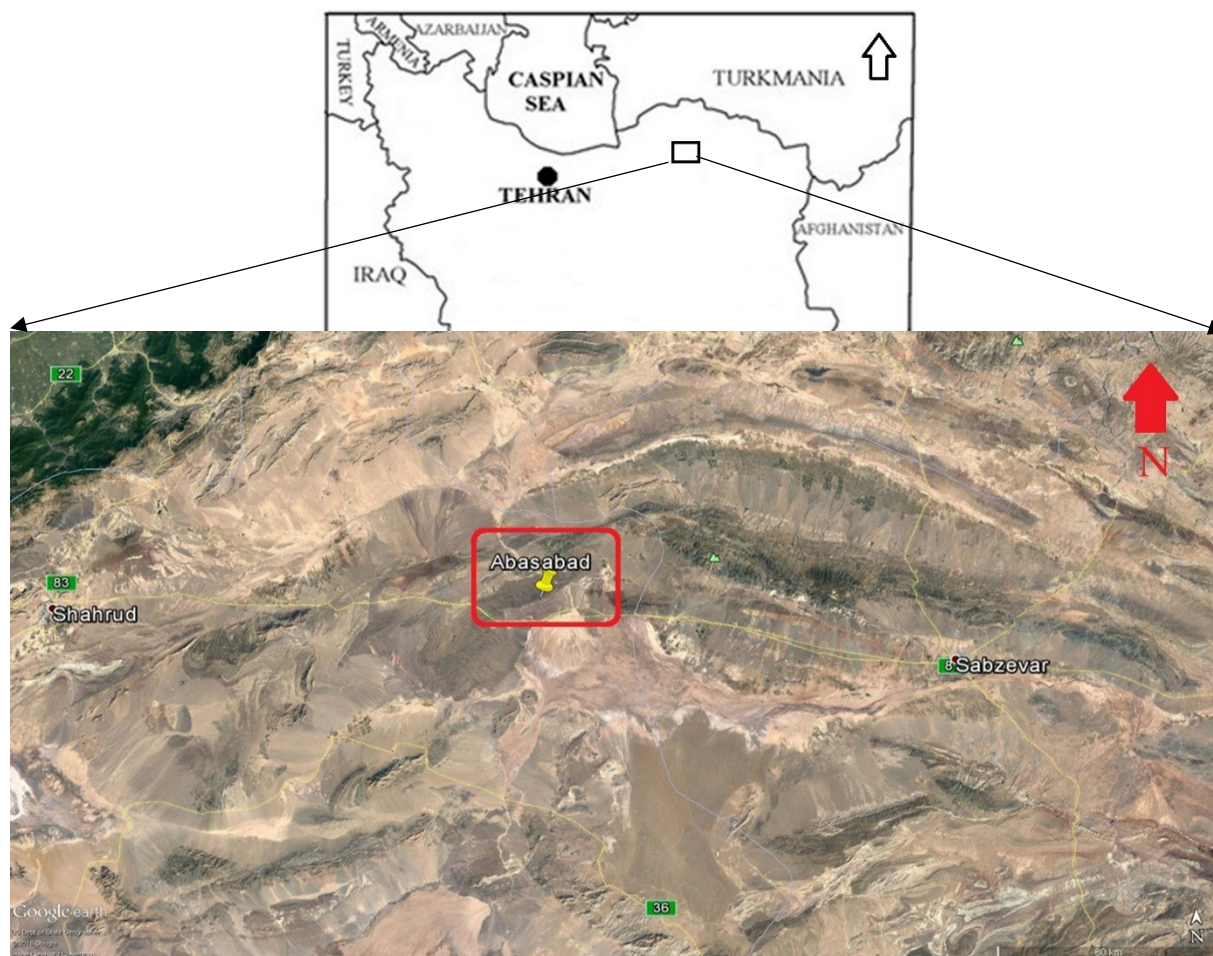


Figure 1. Locations of Madan Bozorg copper mine and Abassabad village in Iran.

**2.2. IP & Rs survey designing and data acquisition**

As mentioned earlier, this work was done to investigate the IP & Rs efficiency in Madan Bozorg so the IP & Rs profiles were designed based on the exploration borehole positions. The geophysical profile position was chosen so that it covers most exploration boreholes. According to the mineralization type, mine situation, and

surveying conditions, the CRSP array was selected for this investigation; CRSP stands for Combined Resistivity Sounding and Profiling. This array is a combination of geoelectrical profiling and sounding, which can lead to useful results in various topographical and geological conditions [4]; for more information, please refer to [3, 12, 24].

Therefore, four profiles were designed and surveyed using the CRSP array (Figure 2). P1 and P2 were surveyed along the borehole profiles with 10 m electrode spacing in the eastern part of the mine. P3 and P4 were surveyed for the evaluation of IP & Rs, and therefore, along these profiles, there were no exploration boreholes. P3 was located 50 m south of P1 and P2, and was also parallel to them. The electrode spacing of P3 was 20 m. P4 was located 500 m from the western part of the others by 10 m electrode spacing. Finally,

2000 points were read in the length of all profiles. The data was collected using a one-channel direct current resistivity and IP WJD-3m (Chongqing Benteng Digital Control Technology Institute). This instrument measures time-domain chargeability in seven windows. For the IP dataset collected here, only the first IP-window was recorded (delay time: 200 ms, integration time: 40 ms). In order to check the data quality, several measurements were randomly repeated in the field.

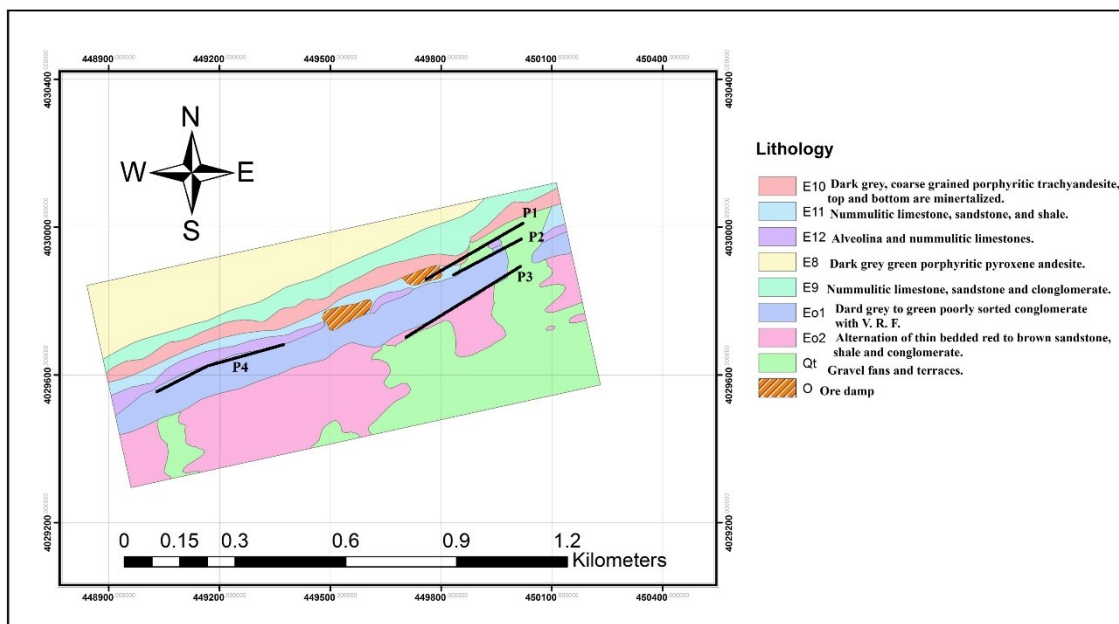


Figure 2. Geological map of Madan Bozorg copper mine.

### 3. Results and discussion

Field surveying and data acquisition were done successfully. The data obtained was revised, the data accuracy was checked, and then data processing was carried out. In the first stage, 2D imaging of the profiles was prepared. Then a 3D model of the data was prepared based on the geostatistical methods. Also for the determination of the IP & Rs data thresholds, the statistical and fractal methods were used. The result of 3D modeling was checked by the geostatistical methods and drilling results.

#### 3.1. IP and Rs data inversion

As mentioned earlier in this paper, the IP & Rs data inversion was done in the first stage, and 2D IP & Rs imaging was carried out. The Rs and IP datasets were inverted using the RES2DINV software [25]. In order to prepare the IP & Rs sections, the Rs and IP datasets were inverted by the Newton and Gauss-Newton methods from the RES2DINV software package [26]. Other options

in RES2DINV were used for inversion but Newton and Gauss-Newton had better results according to the RMS error and geological information, thus these options were selected for the inversion and preparing sections. It is noteworthy that in this research work, the CRSP array was used and there was no option for it in the RES2DINV software package. Thus the free array option from the RES2DINV software package was used, in which the input database of the free array option was different from the other conventional array inputs. In the free array option, the array input of the location of potential and current electrodes for each data-each point that was read-was designated. For this purpose, one location, generally the first potential electrode in the start of profiles, in the length of the profiles was considered to be a base, and then the location of the pair of potential and current electrodes for each data-each point that was read-was calculated relative to the base point. Thus for each point, the location of the pair of potential and current

electrodes and IP & Rs was entered in the database as the software input. The initial damping factor was set to 0.23, and the “L-curve method” option was used to select an optimized damping factor for the subsequent iterations. Regarding the topographic effect, the “distorted grid with damped distortion” option was used to incorporate the topography in the inverse modeling process.

The inversion results and compiled sections are presented as follow:

**Profile 1:** This profile was surveyed in the northern part of the studied area; the profile length was 250 m. In the length of this profile, 9 stations of CRSP were surveyed with NE-SW direction. The results of inverse modeling on the data are shown in Figure 3. The maximum value for chargeability was 45 mv/v, and the maximum value for Rs reached 900  $\Omega$ m. The threshold of IP values was 27 so the values for more than 27 were anomalous, and for the Rs values, the threshold was 300 according to the fractal methods. The maximum depth investigation reached 60 m. In the Rs section, there were two main layers. The first layer with low Rs (less than 300  $\Omega$ m) was related to the sedimentary units. This layer consisted of marl that was more in depth in the surface clay minerals, and by increasing the depth, the limestone increased and clay minerals were reduced. The depth of this layer was various but the average depth was 20 m. In some locations

(from 30 to 80 m of start of profile), the depth of this layer was more than 20 and reached 50 m. The second layer was igneous rocks, especially andesite, which had a high resistivity value (more than 300  $\Omega$ m, up to 900). As mentioned in the geological explanations, mineralization was in the igneous rocks such as andesite. Thus a high Rs value was a potential for mineralization. Based on the IP section, there was a very good mineralization in this profile. At the beginning of the profile to 30 m, there was a mineralization body with an IP value more than 27 up to 38 mv/v, and the depth of this mineral-body was about 25 m and continued to more than 50 m. From 30 to 70 m of the profile, there was no important anomaly. After that, in the depth of about 20 m, there was a good anomaly in all the profiles, in which the thickness was variable from 15 to 50 m. In the 80 m trailing profile, the anomaly was continued up to 50 m and the IP value reached 45 mv/v. As mentioned earlier, over the profile number 1, there were 6 exploratory boreholes. After the study of drilling result and compliance with geophysical sections, there was a very good correlation between them. The drilling results confirmed the geophysical sections, and the geophysical anomalies had a good correlation with the real mineralization. In some locations, the error of anomaly depth estimation was about 3 m.

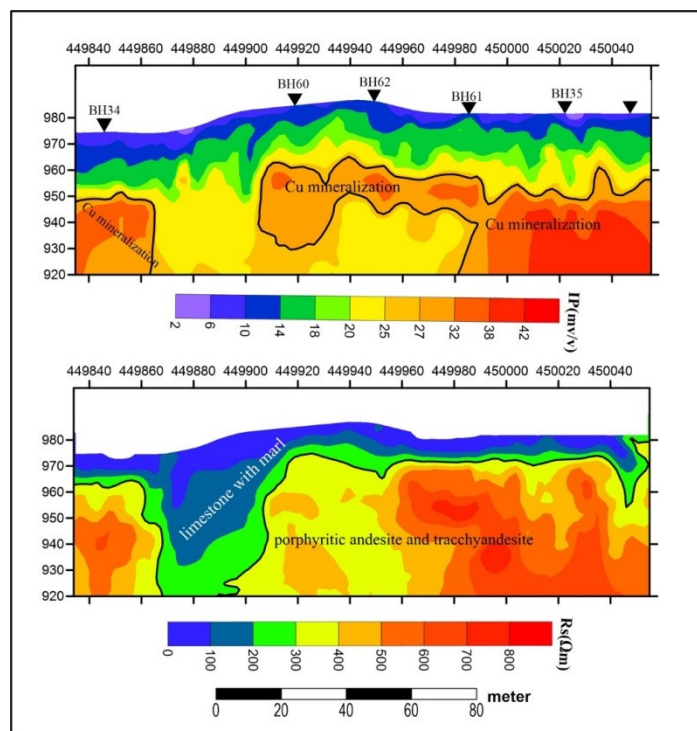
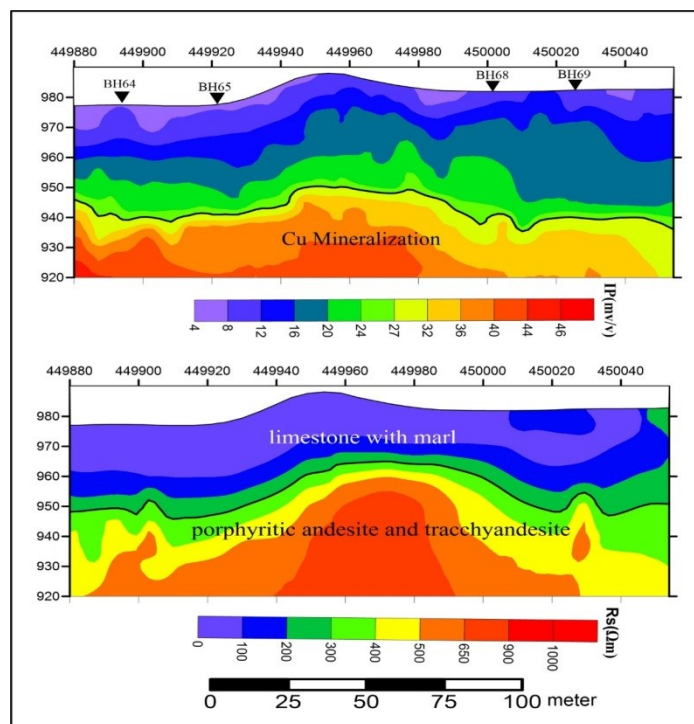


Figure 3. Inverted Rs and IP sections with topography based on data from profile 1 (available exploratory boreholes marked with BH).

**Profile 2:** P2 was surveyed in the south of P1 and parallel to it (NE-SW direction). The length of this profile was 180 m with 6 CRSP stations and 10 m potential electrode spacing. Over this profile, three were 6 exploratory boreholes. The results of inverse modeling of P2 are shown in Figure 4. The maximum values for Rs and IP were 1100  $\Omega$ m and 45mv/v, respectively. The maximum depth investigation for this profile was 70 m. The anomaly threshold (27 for IP and 300 for Rs) is marked in the sections of Figure 4. According to the Rs section from the surface to depth of about 25 m, there was a sedimentary layer consisting of clay mineral and limestone. Rs of this layer was less than 300  $\Omega$ m, and the IP value in this layer was less than 20 mv/v. In this layer, there was no mineralization. Based on these

sections, it can be stated that by increasing the depth, the clay mineral is reduced and the limestone value is increased. Based on the Rs section from the depth of 30 m, of course, in some locations (middle part) of 15 m, igneous rocks begin. According to the IP section, there is an anomaly in all of the profiles from the depth of about 35 or 40 m. This anomaly continues to a maximum depth that can be investigated. By increasing the depth of anomaly, the intensity is increased.

The exploratory borehole of this profile was investigated. The drilling results showed that the geophysical anomaly had a good correlation with the real mineralization. The geophysical sections can detect mineralization as well.



**Figure 4. Inverted Rs and IP sections with topography based on data from profile 2 (available exploratory boreholes marked with BH).**

**Profile 3:** This profile is located in the southern part of the studied area, and it is parallel to P1 and P2. The length of P3 is about 350 m, and 6 CRSP stations were surveyed. There is no topography variation in this profile location. The maximum current length reaches 500 m, the potential electrode spacing is 20 m, and the maximum depth detected is 145 m. The results of inverse modeling of P3 are shown in Figure 5. The maximum IP value is 36 mv/v, and the maximum Rs value is 1100  $\Omega$ m in this profile. From the surface up to about 50 m (max, 50 m), there is a layer with an Rs value less than 100  $\Omega$ m. This

layer is conglomerate, and it has the outcrop in some locations. From a depth of 100 to 120 m, there is a layer with an Rs value of more than 250  $\Omega$ m that continues to the maximum depth. This layer is andesite, which has a mineralization potential. Between these two layers, there is a limestone layer with a little clay mineral that is mentioned in P1 and P2.

According to the IP section, the anomaly values start from an average depth of about 130 m. This anomaly forms a layer that is in the total length of the profile. With respect to the maximum IP value, which is less than P1 and P2 (36 vs. 45),

the threshold value is also less. Thus the threshold value of this profile according to fractal methods is 25 mv/v (Figure 5). As mentioned in the designing part, along the length of this profile does not have any borehole, so based on the geophysical results, two boreholes have been proposed for drilling. The coordinate of the

proposed boreholes includes BH1 (X = 449755; Y = 4029726), BH2 (X = 449919; Y = 4029841). The drilling data obtained confirmed the geophysical results, and there was a good correlation between the geophysical and drilling results.

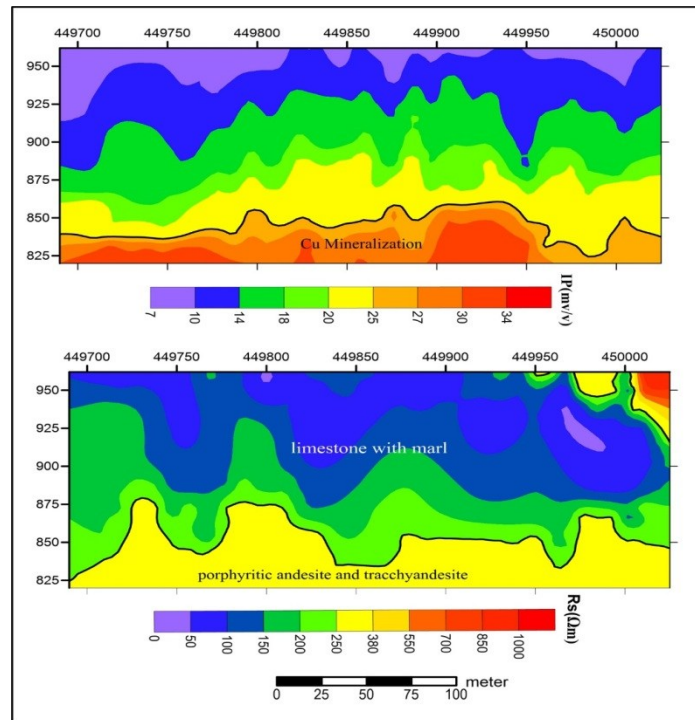


Figure 5. Inverted Rs and IP sections with topography based on data from profile 3.

**Profile 4:** This profile is located in the eastern part of the studied area, and it has more distance compared to the other profiles. The goal of surveying this profile is studying other parts of this mine that have no deep exploration activity, and checking the results obtained in the previous part. This profile has a 360 m length with 12 CRSP station by a potential electrode spacing of 10 m. The results of inverse modeling of P4 are shown in Figure 6. The maximum IP value is 100 mv/v, and the maximum Rs value is 1200  $\Omega$ m in P4 section. Based on the Rs section, similar to P1 and P2, there is a surface layer with an average thickness of about 30 m. Material of this surface layer is marl at the surface, and by increasing the depth, the limestone value is increased. After this surface layer, there is an andesite layer that has a

high Rs value (more than 300  $\Omega$ m). The depth of this layer is various and starts from 20 m, and the maximum depth reaches 50 m (Figure 7). According to the IP section, there is a good anomaly area in this profile that is separated by a black dash in Figure 7. At the beginning of the profile to 50 m and in the depth of 40 m, there is an anomalous body. The biggest anomaly is located at a distance of 150 to 300 m of P4 that has various depths. The minimum depth of this anomaly is 20 m that is located at a distance of 240 m in this section. Based on the geophysical results, 1 exploratory borehole, BH3 (X = 449172; Y = 4029640), has been proposed and derailed that there are good correlations between the geophysical and drilling results.

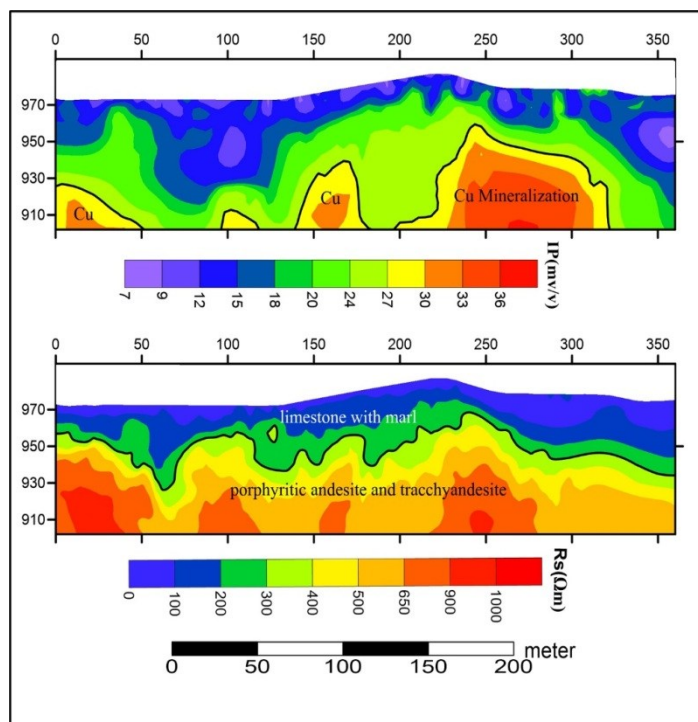


Figure 6. Inverted Rs and IP sections with topography based on data from profile 4.

According to the results obtained from the geophysical study and those related to the drilling data, we can say that the Rs and IP sections and mineralization zones have a rather well agreement with each other. In the profile, location of the mineralization is traced with an acceptable accuracy by high values of Rs and IP. A combination of the drilling and inversion results lead to revealing two main lithology types including the sedimentary and igneous units. The sedimentary units include sandstone and limestone with marl and shale, detected by a low Rs value (less than 300  $\Omega\text{m}$ ) in the Rs section. The igneous rock includes trachyandesite and porphyritic andesite, determined by a high Rs value (more than 300  $\Omega\text{m}$ ) in the Rs sections that have been considered as the host-rocks of the mineralization. The copper mineralization is related to the high IP value determined in the IP section. The efficiency of IP & Rs in the Madan Bozorg copper mine is rather high, and using this investigation can reduce and optimize the drilling operation. For a further investigation and optimization of the exploration boreholes, we need a 3D model of the studied area. By a 3D model, we can have a better view of the area between the profiles and also the studied area.

### 3.2. Preparing 3D models by geostatistical methods

#### 3.2.1. Variography results

In geostatistics, a spatial structure is essential for the use of geostatistical methods. The variogram is a fundamental tool in geostatistics for investigating the spatial structure. As it provides critical parameters for various Kriging estimators, the accuracy of the proposed parameters from the variogram is of crucial importance, and it can have a significant positive or negative influence on the estimated blocks [19]. The variogram provides a lot of information about the parameter under study; they are essentially tools for other geostatistical calculations. One of the possible (and perhaps the most important) uses of the variogram is the estimation of the parameter value at the un-sampled location, and/or estimation of the average over a certain area [27]. The variogram is used to determine the spatial relationship between the regional variables. The variogram is particularly attractive for geoscience engineering because important characteristics of the studied region can be calculated (e.g. range, anisotropy, and continuity). In order to prepare a 3D model in the first stage, variography was done. According to the above factors and applying the related software such as SGeMS [28], the experimental variograms for data were calculated and presented scientifically. Variograms for various parameters such as different azimuth and dip were calculated. The appropriate theoretical models based on the least square differences were fitted to the variogram. For geostatistical estimation, we need 3 variograms perpendicular to

each other that are used in ellipsoid screech. The search radius in the x, y, and z directions is used based on the range of variograms. Thus the theoretical and empirical models of the variogram for data including maximum range, median range, and minimum range that are essential for modeling are presented (Figures 7-9).

As mentioned earlier, these variogram parameters are necessary for modeling. As shown in the Figures 8-10, the Gaussian variogram model is proposed as the best fitted theoretical model. The characteristics of the variogram obtained are presented in Table 1. The minimum range of the variogram is 32 m and a medium obtained is 45 m, while the maximum range is about 70 m.

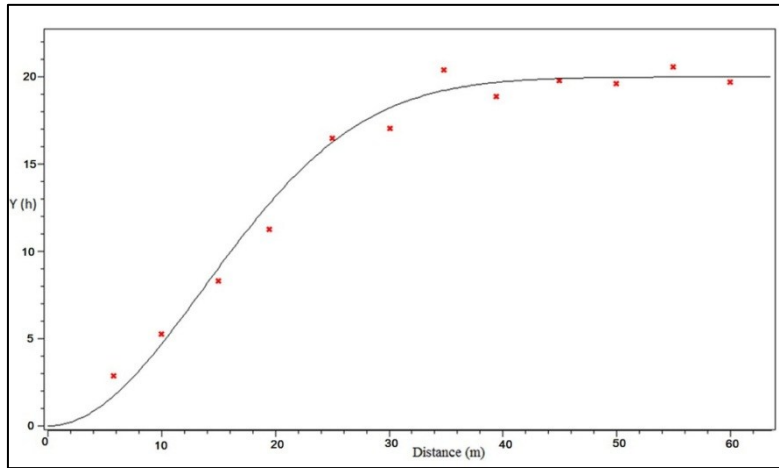


Figure 7. Variogram model for a minimum range of IP data.

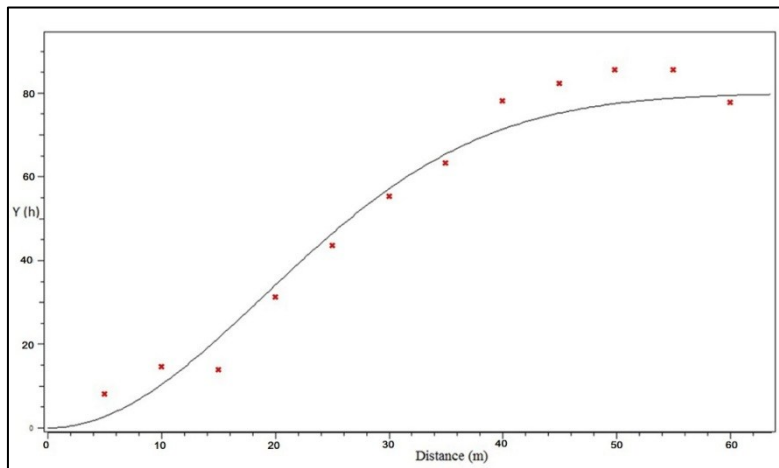


Figure 8. Variogram model for a median range of IP data.

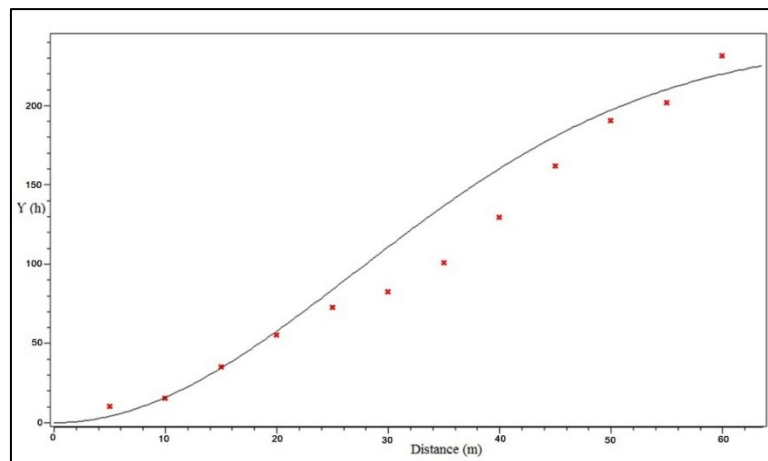


Figure 9. Variogram model for a maximum range of IP data.

**Table 1. Parameters obtained for the presented variogram.**

Azimuth	Dip	Model	Range (m)	Sill (mv/v) <sup>2</sup>	Nugget effect (mv/v) <sup>2</sup>
40	0	Gaussian	32	20	0
30	45	Gaussian	45	80	0
10	45	Gaussian	70	230	0

**3.2.2. Determining uncertainties of fitted variogram**

After variogram fitting and obtaining the variogram parameters, determining the uncertainties of the fitted variogram is required. By the jackknife Kriging method [29], the variogram parameters are obtained and the uncertainties are determined. In the Jackknife analysis, the estimated data is compared against the measured values for a set of locations different from those used as the input data. The calculation of the difference between measured values (experimental) and estimated values in the same points by the Kriging method is introduced as the jackknife error. The average of this error should

be zero and the standard deviation of this error should be minimum [29].

The diagram of the actual values against the estimated values for IP in this work is presented in Figure 10. As shown, these values have a positive correlation (nearly 1). Also for further checking, the histogram of the residual values for the IP data is plotted (Figure 11). The histogram analyses show that the residual value mean and standard deviation are suitable in this work. Based on the diagram and histogram results (Figures 10 and 11), it can be concluded that the variogram parameters have a sufficient accuracy for 3D modeling. It should be noted that since the results for IP and Rs are similar, only the IP results are presented.

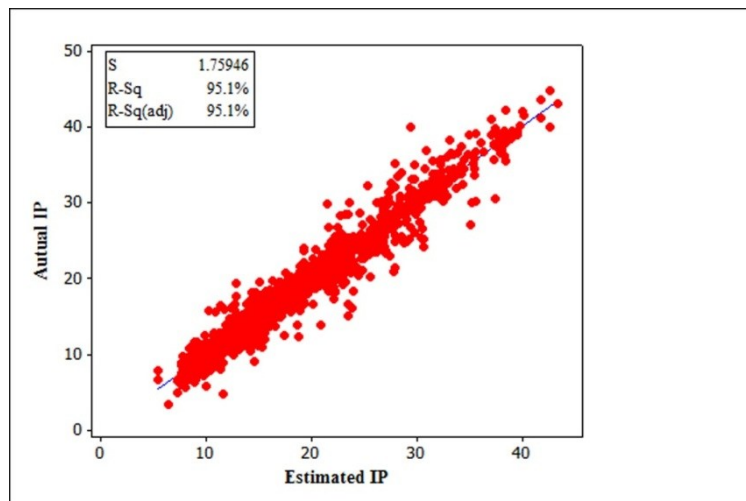


**Figure 10. Diagram of actual values against estimated values of IP data after variography.**

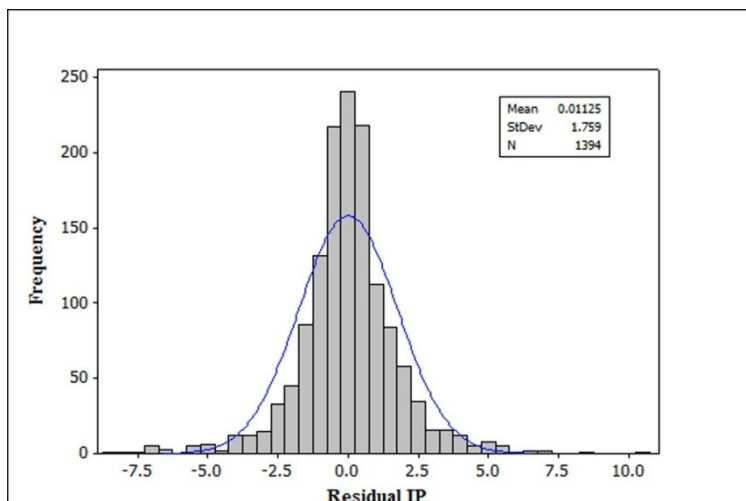


**Figure 11. Histogram of residual values for IP data after variography.**

### 3.2.3. 3D modeling

After variography based on the parameters obtained for the presented variogram, the 3D modeling of data was carried out. The Datamine Studio3 software was used to prepare the 3D models. The input data of the Datamine Studio3 software was the 2D modeling results obtained from inversion. The inversion results of P1, P2, and P3 were used for modeling, and P4 was not used due to more distance for other profiles. The two models presented are IP and Rs as a 3D block model in Figures 12 and 13, respectively. 45 mv/v is the maximum value for IP and 850  $\Omega$ m for Rs. Based on the fractal method analysis of these models, the threshold to IP is 26 mv/v, and the Rs threshold is 250  $\Omega$ m. According to the models (Figures 12 and 13), there is a dominant anomaly in the studied area. The 3D model shows that the anomaly has an almost E-W direction, and it has a

continuous mineral-body. The mineral-body slope is N-S, in which the depth of mineralization in the northern part is about 20 m, and in the southern part, it reaches 130 m. The average thickness of the mineral body is about 25 m. We can reach the mineralization position in each desired location by this 3D model. The drilling plane can be optimized based on these models. In order to evaluate the modeling error as well as the accuracy of the models, the uncertainty was investigated. In order to check the results obtained for the models, we proposed 2 exploration boreholes including BH4 (X = 449882; Y = 4029837) and BH5 (X = 449882; Y = 4029837). These boreholes are located between P2 and P3. The drilling results confirmed the 3D model results. The drilling results are presented in Section 4.4.

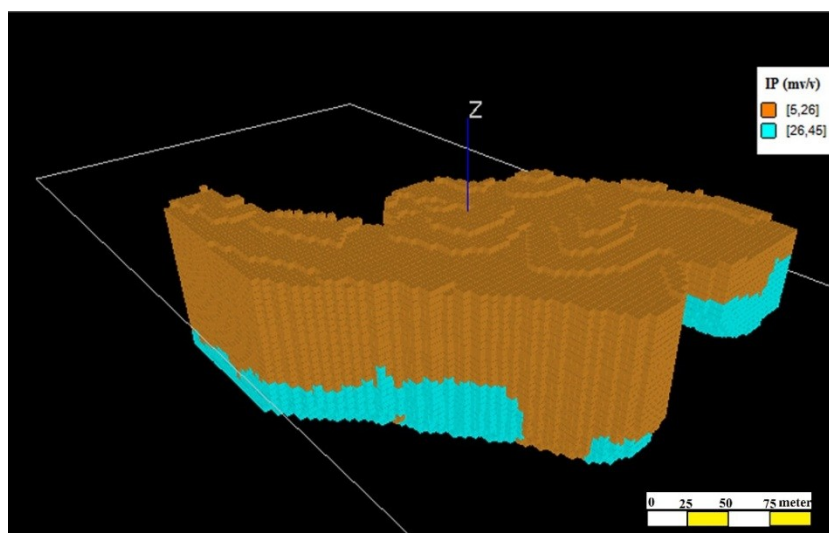


Figure 12. The 3D block model of IP data in Madan Bozorg.

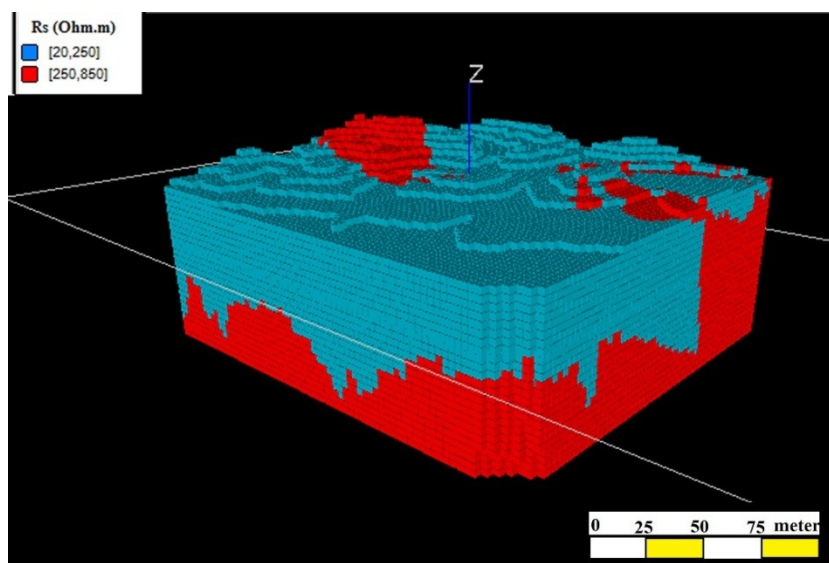


Figure 13. The 3D block model of Rs data in Madan Bozorg.

### 3.3. Uncertainty and validation of estimated values

The Kriging estimation variance (EV) is a measure of uncertainty in predictions, and is a function of the variogram, the sample structure, and the sample support (the area in which an observation is made, which may be estimated as a point or may be an area) [30]. Evaluating EV in each point, which is not dependent on the data value, is one of the main strengths of the geostatistical methods. Moreover, Kriging gives an error distribution as well. EV of each estimated node can be projected by the following equation:

$$\delta_E^2 = 2\gamma(v, V) - \gamma(v, v) - \gamma(V, V) \quad (1)$$

where  $\gamma(v, V)$  is the mean of the variogram (the tail of variogram is fixed on the actual data and its head is fixed on the nodes that should be estimated),  $\gamma(v, v)$  is the mean of the variogram

when the variogram vector's tail and head are fixed on the actual (real) data, and  $\gamma(V, V)$  is the mean of the variogram (head and tail have been fixed on each of the estimated nodes; so for point Kriging, it should be considered as a nugget effect, and for block Kriging, it is estimated by some related functions (e.g. F and H functions)) [30]. The estimation variance of the IP and Rs data was calculated and presented as a distribution 3D block model in Figures 14 and 15, respectively. Due to the standardization of data, the estimation variance value is between 0 and 1. The minimum value for EV indicates that the error of estimation is minimum, and with increase in the amount of EV error, the value of estimation and modeling increase. The results obtained show that the minimum variance is in the profile location, and away from the profiles, the estimation variance is increased.

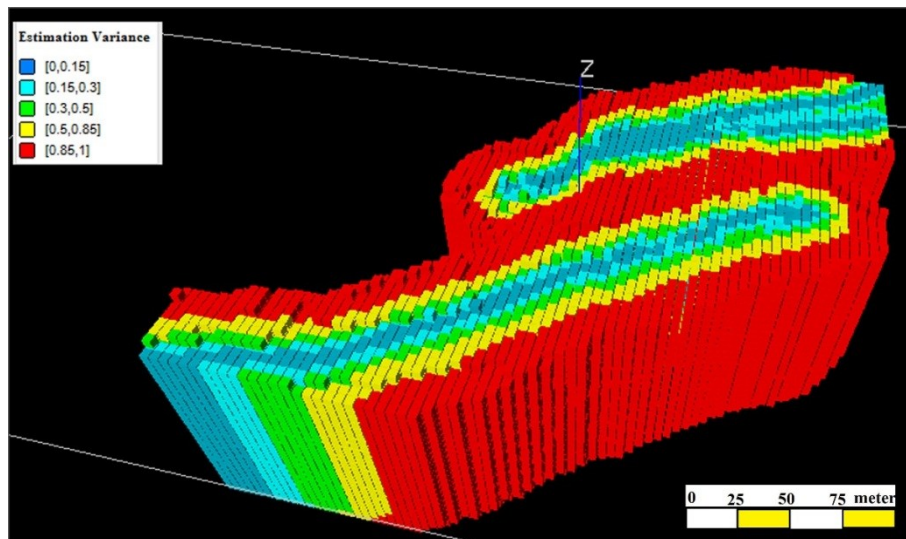


Figure 14. 3D model of estimation variance distortion for IP data.

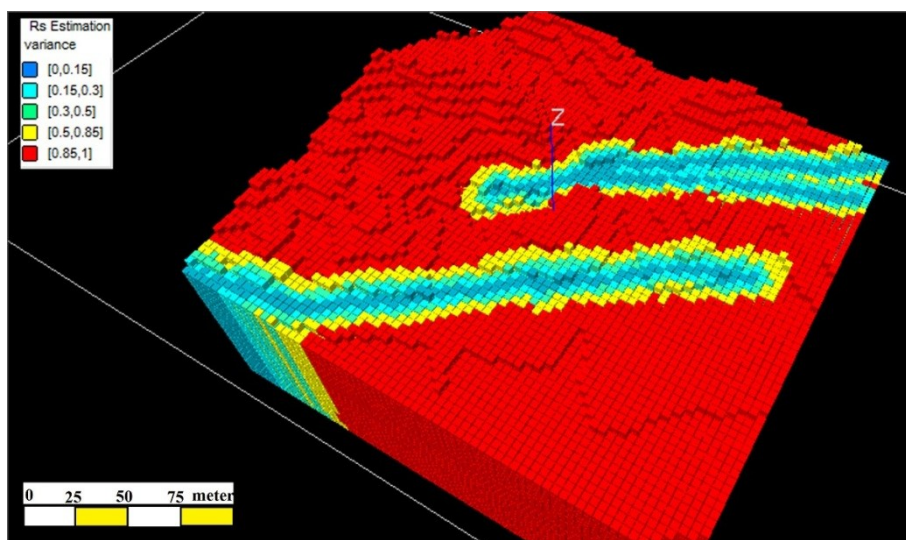


Figure 15. 3D model of estimation variance distortion for Rs data.

The Kriging estimation variance is a good parameter to check the error of estimation but it is not sufficient. The major parameter proposed in Krige (1996) and documented in Snowden (2001) is the “Kriging efficiency”. This is a comparative measure for confidence in the individual block estimate. Thus the Kriging efficiency is the best parameter to check the error of modeling. Also it is of crucial importance to assess the uncertainty of the Kriging evaluation. Therefore, Krige (1996) has presented a practical analysis to assess the spatial continuity and the available data within the search ellipse affecting measures of conditional bias. The parameter called the Kriging efficiency (KE%) has been proposed by Krige (1996) to evaluate the strengths of the Kriging method applied for estimating the grade of each block (i.e. there is an exclusive KE for each block, which can

also be used to calibrate the confidence in block estimates). KE is calculated as Equation (2):

$$KE = (BV - KV) / BV \tag{2}$$

where BV is the theoretical variance of blocks within the domain and KV is the variance between the Kriging grade and true (unknown) grade, i.e. Kriging variance. A perfect estimation would give values of KV = 0 and KE = 100% (Snowden, 2001). The Kriging efficiency of the IP and Rs data in the Madan Bozorg copper mine was calculated. The results of KE for IP and Rs are presented in Figures 16 and 17 as 3D block models. KE is between 0 and 1; the best value for KE is 1, which does not have any error. A zero value for KE is not desirable, and by increasing the KE value, the error value of estimation and modeling is reduced.

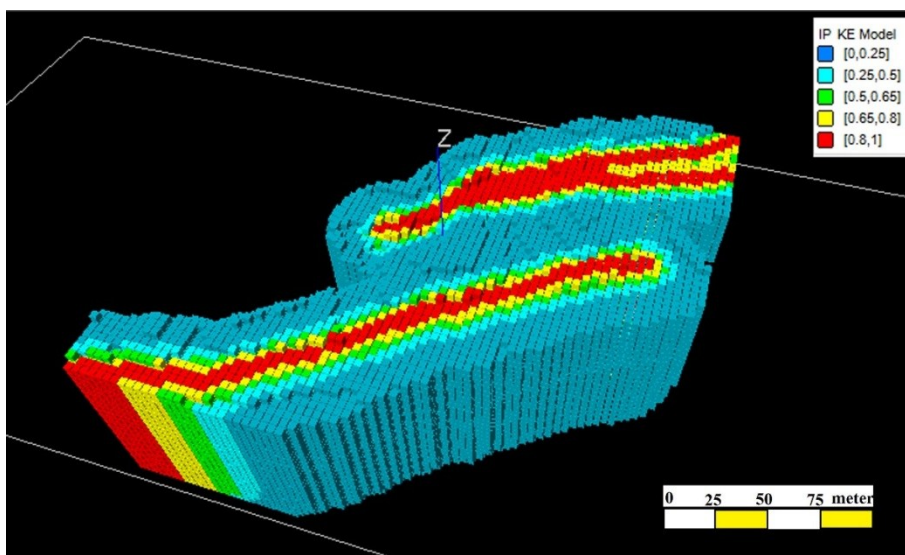


Figure 16. 3D model of KE distortion for IP data.

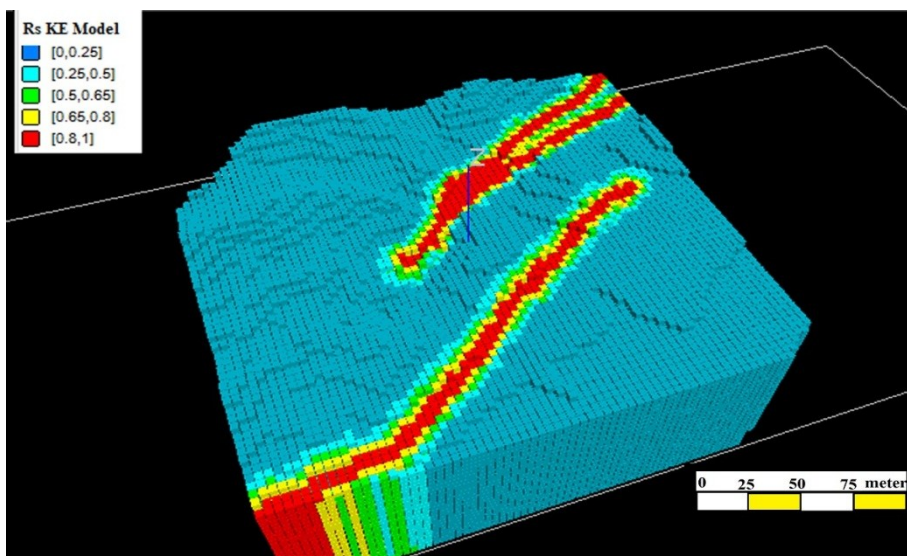


Figure 17. 3D model of KE distortion for Rs data.

### 3.4. Validating model by drilling boreholes

As mentioned earlier, we determined the anomaly values in 2D sections and 3D models. The detected anomaly details such as depth, location, and thickness have been presented in the previous parts (see 4.1 and 4.2.3). Based on the detected anomalies, some locations were selected and proposed for drilling (Figure 18). The proposed boreholes were drilled as core derailing. In the boreholes, cores were collected and classified in

drilling boxes (Figure19). After a primary study of the obtained cores, the probable mineralized cores were analyzed. The drilling results of the three boreholes are presented as example in Tables 2, 3 and 4. In the mentioned tables the depth and the grade of copper are presented in the depth where there is a possibility of mineralization. The results of drillings show that geophysical anomalies have a very good correlation with copper mineralization.

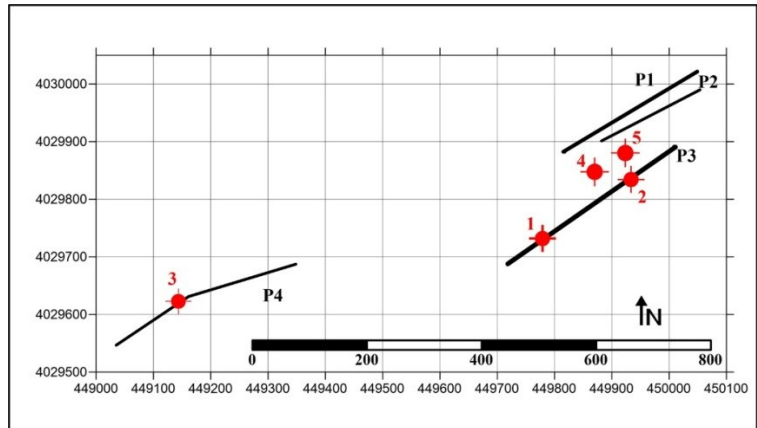


Figure 18. Proposed borehole drilling location in geophysical profile map in the studied area.



Figure 19. Drilling boxes of BH2 in Madan Bozorg.

Table 2. Results of drilling in proposed BH5.

Depth (m)		Cu (ppm)
from	to	
96	98	3357.58
98	100	1727.83
100	102	4098.14
102	104	6976.77
104	106	3552.02
106	108	479.59
108	110	25.46
110	112	540.58
112	114	711.42
114	116	167.5
116	118	928.15
118	120	332.58
120	122	80.27
122	123.9	58.31

Table 3. Results of drilling in proposed BH2.

Depth (m)		Cu (ppm)
from	to	
113.3	114	52.19
114	116	68.96
116	118	13673.86
118	120	92.26
120	122	4121.93
122	124	882.46
124	126	2163.5
126	128	5416.05
128	130	2280.83
130	132	2412.71
132	134	2498.13
134	136	3852.16
136	138	1079.14
138	140	5373.23
140	142	4319.57

Table 4. Results of drilling in proposed BH3.

Depth (m)		Cu (ppm)
from	to	
16	17	464
17	18	334
18	19	357
19	20	1298
20	21	9432
21	22	1583
22	23	1564
23	24	4155
24	25	22474
25	26	5608
26	27	1511
27	28	1796
28	29	1009
29	30	2830
30	31	2352

#### 4. Conclusions

In this work, integration of time-domain induced polarization (IP) and DC-resistivity (Rs) has been successfully used in order to determine the mineralization zone in the Madan Bozorg copper mine. The 2D IP and Rs sections along each one of the profiles was prepared using the inversion method, and the anomaly value was determined in each section.

Based on the IP & Rs results (obtained 2D sections) using geostatistical methods, the 3D models of the IP and Rs data were estimated. For this purpose, in the first stage, the required parameters for modeling were calculated by variography. The validation parameters of the variograms were investigated. 3D block models of IP and Rs were performed; in these models, the IP and Rs parameters were shown with high accuracy, and the mineralization zone was marked in different directions.

To quantifying the uncertainties of the prepared models and evaluation of the modeling error, the estimation variance (EV) and Kriging efficiency (KE) of the models were calculated and presented as 3D models of EV and KE. These models helped us to determine the anomaly zone with less error estimation.

In the determined anomaly zone based on the 2D and 3D models of IP and Rs, 5 exploratory boreholes were suggested and drilled. The results obtained showed that the IP and Rs anomalies had a good conformity with copper mineralization.

According to this modeling, we can reduce the number of boreholes and optimize the exploration borehole pattern. Thus the cost and time of exploration would be reduced and optimized.

#### References

[1]. Gadallah, M.R. and Fisher, R. (2009). Exploration Geophysics. Berlin. Springer. <http://doi.org/10.1007/978-3-540-85160-8>.

[2]. Telford, W.M., Geldart, L.P. and Sheriff, R.E. (1990). Applied Geophysics. Cambridge. Cambridge University Press. <http://doi.org/10.1180/minmag.1982.046.341.32>.

[3]. Ramazi, H. and Mostafaie, K. (2013). Application of integrated geoelectrical methods in Marand (Iran) manganese deposit exploration. Arabian Journal of Geosciences. 6 (8): 2961-2970.

[4]. Mostafaie, K. and Ramazi, H. (2015). Application of electrical resistivity method in sodium sulfate deposits exploration, case study: Garmab, Iran. Journal of Biodiversity and Environmental Sciences. 6 (2): 2220-6663.

[5]. Sultan, S.A., Mansour, S.A., Santos, F.M. and Helaly, A.S. (2009). Geophysical exploration for gold and associated minerals, case study: Wadi El Beida area, South Eastern Desert, Egypt. Journal of Geophysics and Engineering. 6 (4): 345-356.

[6]. Ferdows, S.M. and Ramazi, H. (2015) Application of the fractal method to determine the membership function parameter for geoelectrical data (case study: Hamyj copper deposit, Iran). Journal of Geophysics and Engineering. 12 (1): 909-921.

[7]. Yang, J., liu, Z.H. and Wang, L. (2008). Effectiveness of Natural Field Induced Polarization for Detecting Polymetallic Deposits. Earth Science Frontiers. 15 (4): 217-221.

[8]. Flores, C. and Peralta-Ortega, S.A. (2009). Induced polarization with in-loop transient electromagnetic soundings: A case study of mineral discrimination at El Arco porphyry copper, Mexico. Journal of Applied Geophysics. 68 (3): 423-436.

[9]. Mammo, T. (2009). Geophysical Models for the Cu-Dominated VHMS Mineralization in Katta District, Western Ethiopia. Natural Resources Research. 22 (1): 5-18.

[10]. Kozhevnikov, N.O., Antonov, E.Y., Zakharkin, K. and Korsakov, M. (2014). TEM surveys for search of taliks in areas of strong fast-decaying IP effects. Russian Geology and Geophysics. 55 (12): 1452-1460.

[11]. Gurin, G., Tarasov, A., Ilyin, Y. and Titov, K. (2015). Application of the Debye decomposition approach to analysis of induced-polarization profiling data (Julietta gold-silver deposit, Magadan Region). Russian Geology and Geophysics. 56: 1757-1771.

[12]. Mashhadi, S.R., Mostafaei, K. and Ramazi, H.R. (2017). Improving bitumen detection in resistivity surveys by using induced polarization data. Exploration Geophysics. Published online: <https://doi.org/10.1071/EG17032>.

[13]. Doulati Ardejani, F., Jodeiri Shokri, B., Moradzadeh, A., Soleimani, E. and Jafari, M.A. (2008). A combined mathematical geophysical model for prediction of pyrite oxidation and pollutant leaching associated with a coal washing waste dump. International Journal of Environmental Science and Technology. 5 (4): 517-526.

[14]. Rucker, D.F., Glaser, R.D., Osborne, T. and Maeh, W. (2009). Electrical Resistivity Characterization of a Reclaimed Gold Mine to Delineate Acid Rock Drainage Pathways. Mine Water Environment. 28: 146-157.

[15]. Gomez, E.P., Parviainen, A., Hokkanen, T. and Ruskeeniemi, K.L. (2010). Integrated geophysical and geochemical study on AMD generation at the Haveri Au-Cu mine tailings, SW Finland. Environmental Earth Science. 1: 1435-1447.

- [16]. Jodeiri Shokri, B., Doulati Ardejani, F. and Moradzadeh, A. (2016). Mapping the flow pathways and contaminants transportation around a coal washing plant using the VLF-EM, Geo-electrical and IP techniques-A case study, NE Iran. *Environmental Earth Sciences*. 75 (1): 1-13.
- [17]. Gazoty, A., Fiandaca, G., Pedersen, J., Auken, E., Christiansen, A.V., Pedersen, J.K. and Syddanmark, R. (2012). Application of time domain induced polarization to the mapping of lithotypes in a landfill site. *Hydrology and Earth System Science*. 16: 1793-1804.
- [18]. Bourges, M., Mari, J. and Jeann, N. (2012). A practical review of geostatistical processing applied to geophysical data: methods and applications. *Geophysical Prospecting*. pp. 1-13. doi: 10.1111/j.1365-2478.2011.00992.x.
- [19]. Mostafaie, K., Ramazi, H. and Jalali, M. (2014). Application of Integrated Geophysical and Geostatistical Methods in Amiriyeh Site Classification. *Geodynamics Research International Bulletin (GRIB)*. 2 (2): 1-15.
- [20]. Kumar, D., Ahmed, S., Krishnamurthy, N.S. and Dewandel, B. (2007). Reducing ambiguities in vertical electrical sounding interpretations: A geostatistical application. *Journal of Applied Geophysics*. 62 (1): 16-32.
- [21]. Vesnaver, A., Bridle, R., Henry, B., Ley, R., Rowe, R. and Wyllie, A. (2006). Geostatistical integration of near-surface geophysical data. *Geophysical Prospecting*. 54 (6): 763-777.
- [22]. Morari, F., Castrignano, A. and Pagliarin, C. (2009). Application of multivariate geostatistics in delineating management zones within a gravelly vineyard using geo-electrical sensors. *Computers and Electronics in Agriculture*. 68 (1): 97-107.
- [23]. Huang, J., Zhao, B., Chen, Y. and Zhao, P. (2010). Bidimensional empirical mode decomposition (BEMD) for extraction of gravity anomalies associated with gold mineralization in the Tongshi gold field, Western Shandong Uplifted Block, Eastern China. *Computers and Geosciences*. 36 (7): 987-995.
- [24]. Ramazi, H. and Jalali, M. (2014). Contribution of geophysical inversion theory and geostatistical simulation to determine geoelectrical anomalies. *Studia Geophysica et Geodaetica*. 59 (1): 97-112.
- [25]. Loke, M.H. and Barker, R.D. (1996). Rapid least-squares inversion of apparent resistivity pseudosections by a quasi-Newton method. *Geophysical Prospecting*. 44 (1): 131-152.
- [26]. Loke, M.H. and Dahlin, T. (2002). A comparison of the Gauss-Newton and quasi-Newton methods in resistivity imaging inversion. *Journal of applied geophysics*. 49 (1): 149-162.
- [27]. Zawadzki, J. and Fabijańczyk, P. (2007). Use of variograms for field magnetometry analysis in Upper Silesia Industrial Region. *Studia Geophysica et Geodaetica*. 51(4): 535-550
- [28]. Bohling, G. (2007). S-GeMS Tutorial Notes in Hydrogeophysics: Theory, Methods, and Modeling, Boise State University, Boise, Idaho.
- [29]. Lamorey, G. and Jacobson, E. (1995). Estimation of Semivariogram Parameters and Evaluation of the Effects of Data Sparsity. *Mathematical Geology*. 27 (3): 327-358.
- [30]. Journel, A.G. and Huijbregts, C.H.J. (1978). *Mining Geostatistics*, Centre de Geostatistique Fontainebleau. France.

## ساخت مدل سه‌بعدی داده‌های پلاریزاسیون القایی و مقاومت ویژه الکتریکی همراه با کمی‌سازی عدم قطعیت‌ها با استفاده از روش‌های زمین‌آماری و حفاری (مطالعه موردی: معدن بزرگ، ایران)

کامران مصطفائی و حمیدرضا رمضی\*

دانشکده مهندسی معدن و متالورژی، دانشگاه صنعتی امیرکبیر، ایران

ارسال ۲۰۱۸/۳/۳، پذیرش ۲۰۱۸/۶/۳

\* نویسنده مسئول مکاتبات: ramazi@aut.ac.ir

---

### چکیده:

معدن بزرگ یک معدن فعال مس بوده که در شمال شرق ایران واقع شده و بخشی از یک زون بزرگ کانی‌سازی مس به نام کمر بند میامی- سبزواری است. هدف اصلی این پژوهش تهیه مدل سه‌بعدی داده‌های مقاومت ویژه الکتریکی و پلاریزاسیون القایی همراه با کمی‌سازی عدم قطعیت‌ها با استفاده از روش‌های زمین‌آماری و حفاری است. بر اساس داده‌های حفاری چهار پروفیل طراحی و برداشت شد. داده‌های به دست آمده پردازش شده و با استفاده از مدل‌سازی معکوس مقاطع دوبعدی IP,RS برای هر پروفیل تهیه شد و سپس مقاطع تهیه شده با استفاده از داده‌های حفاری ارزیابی شدند. با استفاده از روش‌های زمین‌آماری مدل بلوکی سه‌بعدی داده‌های دوبعدی IP,RS تهیه شد همچنین عدم قطعیت این مدل‌ها محاسبه شد. بر اساس آنومالی‌های به دست آمده محل زون‌های کانی‌سازی تعیین شد. برای ارزیابی مدل‌های به دست آمده در محل‌هایی که حفاری وجود نداشت، چند گمانه اکتشافی برای حفاری پیشنهاد شد. نتایج حفاری دلالت بر این دارد که آنومالی‌های ژئوفیزیکی تعیین شده انطباق بسیار خوبی با زون‌های کانی‌سازی در گمانه‌های حفاری دارد. نتایج به دست آمده نشان داد که تهیه یک مدل سه‌بعدی از داده‌های برداشت شده دوبعدی IP,RS با میزان خطای قابل قبول امکان‌پذیر است. با استفاده از این روش محل بهینه گمانه‌های حفاری تعیین شده و گمانه‌های اضافی حذف می‌شوند همچنین می‌توان مطالعات اکتشافی کانسار مس را با کمترین تعداد گمانه حفاری انجام داد.

**کلمات کلیدی:** مدل سه‌بعدی، پلاریزاسیون القایی، مقاومت ویژه الکتریکی، زمین‌آمار، عدم قطعیت، حفاری.

---